Robust Consensus-Based Formation Control of a Group of UAV

Kaan Can, Abdullah Basci*
Department of Electrical and Electronics Engineering, Ataturk University, 25240, Erzurum, Turkey
*kaan.can@atauni.edu.tr, *abasci@atauni.edu.tr*

***Abstract*—Consensus-based formation control (CFC) is one of the most phenomenal formation control methods designed to achieve consensus between any vehicles using and sharing their position and/or linear velocity with each other in a swarm mission. In this paper, a robust CFC (R-CFC) is designed and proposed to realise predefined formation shapes with a team of unmanned aerial vehicles (UAVs). First, the dynamics of a double integrator of an UAV is presented. Second, graph theory is explained briefly to understand any adjacency between UAVs. Then, the proposed R-CFC algorithm is derived and the stability analysis is proven via algebraic Riccati stability theory based on Lyapunov stability theorem. After that, the effectiveness of the proposed controller is tested in real-time outdoor tests. The experimental results show that UAVs are able to create the desired formation shapes and are less affected by external disturbances such as wind thanks to the proposed control algorithm.**

***Index Terms*—Consensus control; Formation control; Robust control; UAV.**

I. INTRODUCTION

Formation control is a kind of swarm application for some unmanned vehicles to create some special shapes to use different missions. Due to instant information sharing between the swarm members required by formation control, swarm applications are generally carried out with a certain formation control method [1]–[4]. Some of these methods generally used in real-time applications and simulation studies are decentralised control, consensus control, leader-follower and distributed formation control, etc. Basically, the formation control methods mentioned are based on the use of the UAV's positions and/or linear velocities in the swarm to form any predefined shape. In the following paragraphs, literature studies of the control methods mentioned in real-time or simulation studies with UAVs are presented.

Can and Basci [5] studied a leader-follower (L-F)-based formation control in a group of UAVs. The proposed control method has been applied slightly different from the classical L-F method. They applied the L-F formation control by creating a virtual leader to provide trajectory information to the follower UAVs by taking into account the safety distance between vehicles. The simulation results showed that the L-F formation performed with the virtual leader was successfully tracked by the followers. Fathian, Summers, and Gans [6] presented a distributed formation control for a team of UAVs. First, they introduced the linearised model of a four-rotor UAV. Then, the single integrator dynamics of the UAV was derived to apply the proposed distributed controller. To ensure the robustness of the distributed formation controller, a semidefinite programming (SDP) method was used to find formation control gains. The simulation results showed that the proposed control method allows the agents to move along the directed control direction. Toksoz, Oğuz, and Gazi [7] proposed a hybrid decentralised formation control for a group of quadrotor helicopters. In addition, a collision avoidance algorithm was added to the hybrid formation controller to prevent the UAVs from colliding with each other during formation flight. The authors proved the stability of the proposed hybrid controller considering the single integrator dynamics of the quadrotor. Simulation and real-time tests enabled the quadrotors to follow the predefined trajectory successfully, thanks to the proposed control method, and there were no collisions during the formation flight. Thien and Kim [8] proposed two different decentralised formation control technics such as proportional-integral-derivative (PID) and integral sliding mode control (ISMC) to compare disturbance rejection performances. First, they applied the PID-based formation controller under constant input disturbances. The ISMC-based formation controller was then used to address time-varying input disturbances. The experimental results showed that the ISMC-based controller is more robust than the PID-based controller in terms of disturbance rejection characteristic.

Dong, Yu, Shi, and Zhong [9] investigated and designed consensus-based formation control (CFC) to realise a time-varying formation on five quadrotors. First, to achieve predefined time-varying formations, even if the velocities of the quadrotors are different, the proposed control protocol was presented to maintain the formation throughout the time-varying formation flight. The proposed theory for obtaining a time-varying formation was validated with five quadrotors in an outdoor experiment, and its effectiveness was successfully tested. Can and Basci [10] proposed CFC to perform a swarm control for a group of UAVs. The main idea was to create a pentagonal formation along the time-varying trajectory based on the double integrator dynamics of the UAV. Thus, the aim was to provide the desired pentagonal formation owing to instant information sharing between the UAVs. After a successful pentagonal formation

Manuscript received 11 February, 2023; accepted 14 April, 2023.

shape was achieved, it was observed that the UAVs reached a consensus on their linear velocity.

In this paper, the R-CFC algorithm is derived with the help of linear algebra and graph theory and its mathematical analysis is performed. Then, the stability analysis of the proposed formation control method is proved by Lyapunov stability theory. Then, the proposed control method is tested in real time with four open-source UAVs for various formation shapes. The experimental results show that the R-CFC is able to keep the UAVs in the desired formation shapes defined in Fig. 2 and also provides a consensus on the positions of the UAVs.

II. MATHEMATICAL MODEL OF UAV

An UAV can be designed with different configurations such as quadrotor, hexacopter, octocopter, etc. In this paper, the X-type quadrotor is designed and configured to test the proposed control algorithm. An UAV can control by dividing its dynamic structure into two subsystems described as inner-loop control (where the attitude control is realised) and outer-loop control (where the altitude control is realised), respectively. In addition, an UAV has six degrees of freedom and its mathematical expressions can be defined as follows [11], [12]:

$$\begin{cases} \ddot{x} = \dfrac{u_1}{m}(\cos\psi \sin\theta \cos\varphi + \sin\psi \sin\varphi), \\ \ddot{y} = \dfrac{u_1}{m}(\sin\psi \sin\theta \cos\varphi - \cos\psi \sin\varphi), \\ \ddot{z} = \dfrac{u_1}{m}(\cos\theta \cos\varphi) - g, \\ \ddot{\varphi} = \dfrac{(I_{yy} - I_{zz})\dot{\theta}\dot{\psi}}{I_{xx}} + \dfrac{u_2}{I_{xx}} + \dot{\theta}\dot{\psi}, \\ \ddot{\theta} = \dfrac{(I_{zz} - I_{xx})\dot{\psi}\dot{\varphi}}{I_{yy}} + \dfrac{u_3}{I_{yy}} - \dot{\psi}\dot{\varphi}, \\ \ddot{\psi} = \dfrac{(I_{xx} - I_{yy})\dot{\psi}\dot{\varphi}}{I_{zz}} + \dfrac{u_4}{I_{zz}} + \dot{\varphi}\dot{\theta}, \end{cases} . \quad (1)$$

where m represents the mass of the UAV, u_n represents the control input, g represents the gravitational acceleration, and $I_{xx}, I_{yy}, and\ I_{zz}$ represent the inertia matrix of the UAV through the x, y, and z axes, respectively. During formation flights, the dynamics of the outer loop of all the swarm members is controlled, and thus these dynamics can be defined as follows [9]:

$$\begin{cases} \dot{x}_i(t) = v_i(t), \\ \dot{v}_i(t) = u_i(t), \end{cases} \quad (2)$$

where i represents the number of UAVs, $x_i(t) \in \Re^m$ and $v_i(t) \in \Re^m$ represents the position and linear velocity of UAV i, and $u_i(t) \in \Re^n$ represents the control input of UAV i.

III. CONTROLLER DESIGN

In this section, the proposed control algorithm is derived mathematically.

A. Graph Theory

Basically, graph theory is used to describe the interaction of an UAV in contact with its neighbours so as to realise the formation swarm in this paper. Thus, it is assumed that the graph G is an undirected-connected graph and the UAVs are sharing their state information instantly with each other by using a communication system as well.

The graph G includes two basic concepts: the set of nodes (H) and the set of edges (E). H represents the set of nodes $H = \{h_1, h_2, ..., h_n\}$ and $E = \{e_1, e_2, ..., e_n\}$ represents the set of edge graphs $G = (H, E)$.

The number of edges that exit the node expressed by $h_i \in H$, is called the "degree of $h_i \in H$" in that graph and it is a diagonal matrix written as $D(G) = diag[d_1, d_2, d_3, ..., d_n]$. The following expression can be used to find the degree matrix of the graph (G) [13]

$$D(G) = d_i = \begin{cases} \sum_{j=1}^{N} a_{ij}, & if\ \ i = j, \\ 0, & otherwise. \end{cases} \quad (3)$$

Additionally, if there is an edge connecting two nodes in the G, these two points are called "adjacent" and are expressed as $i \neq j \in A(G)$. Here, $A(G)$ represents the adjacency matrix that shows all the neighbours of a graph G structure with n elements and can also be expressed as given below

$$A(G) = \left[a_{ij} \right]_{nxn} = \begin{cases} 1, & if\ \ i \neq j, \\ 0, & otherwise. \end{cases} \quad (4)$$

Using all this information, the Laplacian matrix can be obtained using the differences of the degree matrix given in (3) and the adjacency matrix given in (4) such as $L(G)$ = $D(G)$ - $A(G)$ and can be defined as given in the following [13]

$$L(G) = \left[l_{ij} \right]_{nxn} = \begin{cases} d_i, & i = j, \\ -1, & i \neq j, \\ 0, & otherwise. \end{cases} \quad (5)$$

The matrix $L(G)$ defined in (5) is a symmetric matrix and the sum of its rows and columns is zero.

B. Consensus Controller Design

Let us consider a linear system as given in (6). Here, A and B are both stabilizable [14], [15]

$$\dot{x}_i(t) = Ax_i(t) + Bu_i(t), \quad (6)$$

where $x_i \in \Re^n$, $A \in \Re^{nxn}$, $B \in \Re^{mxn}$, and $u_i \in \Re^m$ are defined. Furthermore, the basic consensus algorithm known in the literature can be written as follows [14], [15]

$$u_i = K \sum_{j=1}^{n} \left[(x_i - x_j) \right]. \quad (7)$$

By using (6), $u(t) = -Kx(t)$ (state feedback) can be

obtained. In all these expressions, the equation given in (6) can be rewritten as the Kronecker product as follows [16]

$$\dot{x}(t) = (I \otimes A)x(t) + (I \otimes B)u(t), \tag{8}$$

where the control signal can be obtained as $u(t) = -(L \otimes K)x(t)$. Moreover, L represents the Laplacian matrix. To obtain the closed-loop expression of the system given in (6) via L, one can write as the following expression, clearly

$$\dot{x}(t) = \left[I \otimes A - (L \otimes BK)\right]x(t). \tag{9}$$

The solution of the expression in (9) is as follows

$$x(t) = e^{[I \otimes A - (L \otimes BK)]t}\, x(0). \tag{10}$$

Expression $x(0)$ denotes the initial states of the vehicles in the swarm. The exponential expression given in (10) can be rewritten as given below

$$e^{[I \otimes A - (L \otimes BK)]t} = (P \otimes I)e^{[I \otimes A - (J \otimes BK)]t}(P^{-1} \otimes I). \tag{11}$$

The Jordan canonical form can be expressed as $J = P^{-1}LP = diag\{0, \lambda_2, \lambda_3, ..., \lambda_n\}$ ($\lambda_2 \rightarrow$ is the smallest eigenvalue of J), where $P > 0$ is a symmetric matrix and contains eigenvectors. The exponential expression in (11) can be rearranged with the help of the Kronecker product as follows [14]

$$I \otimes A - (PJP^{-1}) \otimes BK = \\ = (P \otimes I)(I \otimes A)(P^{-1} \otimes I) - (P \otimes I)(J \otimes BK)(P^{-1} \otimes I). \tag{12}$$

The above equation is more simply rewritten as [17]

$$I \otimes A - (PJP^{-1}) \otimes BK = \\ = (P \otimes I)\left[I \otimes A - J \otimes BK\right](P^{-1} \otimes I). \tag{13}$$

Moreover, considering the property of the P matrix such as $(P^{-1} \otimes I) = (P \otimes I)^{-1}$, as well as using the property of $e^{PBP^{-1}} = Pe^{B}P^{-1}$, the following equation is obtained [15]

$$I \otimes A - J \otimes BK = diag\{A, A - \lambda_2 BK, ..., A - \lambda_n BK\}. \tag{14}$$

The system given in (9) has an undirected and connected graph structure. Also, since the elements of matrix A are fixed, their eigenvalues are constant. Therefore, the consensus design should be achieved with the design of the K gain. In order to design consensus control via the Riccati equation, the appropriate K gain can be chosen as in (15) by using the equation $PA + A^T P - \lambda_2 PBB^T P + Q = 0$ as given below, where A, B are stabilizable and $Q, P > 0$ [14], [15]

$$K = \frac{1}{2}B^T P. \tag{15}$$

Lemma 1: If all eigenvalues of matrix A are negative real parts, the relationship between A and P matrix can be written as $PA + A^T P < 0$ (see for more information in Appendix A). All these steps, Lemma 1 and the Riccati equation, yield the following equation

$$(\lambda_2 - \lambda_n)PBB^T P - Q < 0. \tag{16}$$

From (16), one can understand that the system is stable due to the $\lambda_2 < \lambda_n$ expression. In the light of this information, the proposed R-CFC structure for each UAV in the swarm is obtained as given below [14], [15]

$$u_{fp} = -K\sum_{j=1}^{n}\alpha_{ij}\left[\beta(x_i - x_j - \delta_{ij})\right], \tag{17}$$

where $\beta = 1.5$ represents the gain in position controller tuning and is determined by the trial and error method. Also, the desired formation distance between two UAVs is defined as $\delta_{ij} = \delta_i - \delta_j$. Considering this equality in the proposed consensus equation, for all initial position and linear velocity of each UAV, if $t \rightarrow \infty$, then $\left\|x_i - x_j\right\| \rightarrow \delta_{ij}$. Moreover, to realise more precise formation control, we added an additional control signal to the main formation controller u_{fp} by taking into account the linear velocities of the UAVs as given below

$$u_{fv} = -\chi\sum_{j=1}^{n}\alpha_{ij}\left[\gamma(v_i - v_j - \dot{\delta}_{ij})\right], \tag{18}$$

where $\chi = 1$, and for the success of any formation, $\left\|v_i - v_j\right\| \rightarrow \dot{\delta}_{ij}$ must be satisfied and then the consensus condition within the swarm is fulfilled [14], [15].

C. Collision Avoidance

During a real-time formation flight, to ensure flight safety, a collision avoidance algorithm is added to the expression in (17) and (18) to prevent UAVs from colliding in the air. For this method, the Repellent Morse Potential methodology is used to realise a safe formation flight given in (19) [7]

$$u_{ij}^{r} = \begin{cases} a(e^{-\eta\left\|r_{ij}\right\|} - e^{-\eta\left\|r_s\right\|}), & if\ \left\|r_{ij}\right\| \le r_s, \\ 0, & otherwise, \end{cases} \tag{19}$$

where $a > 0$ represents the control gain, $\eta > 0$ represents the exponential scale, r_{ij} is the measured distance between UAVs, and r_s is the desired safety distance between the UAVs, respectively.

D. R-CFC with Collision Avoidance Algorithm

In this paper, in addition to the R-CFC design, the collision avoidance algorithm is applied to all swarm members with the main formation controller to prevent any collisions in the swarm. Therefore, the total control signal can be written as follows

$$u = u_{fp} + u_{ij}^{r} + u_{fv}. \tag{20}$$

IV. EXPERIMENTAL RESULTS

In this section, we present the experimental results of formation flights. The experiment was carried out in a football stadium. Also, to obtain control parameters, gain matrix A and input matrix B are taken as $A=\begin{bmatrix}0 & 1\\ 0 & 0\end{bmatrix}$, $B=\begin{bmatrix}0\\ 1\end{bmatrix}$, respectively. Moreover, the control parameter given in (15) and P matrix are obtained by using the LMI toolbox of MATLAB as $K=\begin{bmatrix}0 & 0.55395\end{bmatrix}$, $P=\begin{bmatrix}0 & 0\\ 0 & 1.1079\end{bmatrix}$, respectively. In addition, the images of the UAVs, router, and ground control station (GCS) used in the experimental studies are presented in Fig. 1.

Fig. 1. Experimental setup used in the UAV swarm application.

Also, the IP list of all experimental equipment is presented in Table I.

TABLE I. THE EXPERIMENTAL EQUIPMENT LIST.

Number	Name	IP No.
1	Router	192.168.1.1
2	GCS	192.168.1.3
3	UAV 1	192.168.1.11
4	UAV 2	192.168.1.12
5	UAV 3	192.168.1.13
6	UAV 4	192.168.1.14

The hardware features of the experimental setup given in Fig. 1 are as follows: the GCS has an i5 processor, 8 GB ram, and UBUNTU 18.04.6 LTS operating system. Moreover, the UAVs have Raspberry Pi 3-4 main boards to run Python codes and Pixhawk 2.4.8 flight control card. To provide communication between GCS and UAVs, the TCP/IP communication protocol is preferred to provide more secure (peer-to-peer) communication between the equipment.

In Fig. 2, the predefined formation shapes that the UAVs will perform during a formation flight are presented. The first formation shape is a triangular-shape formation. When obtaining this formation, the distance between UAV1–UAV4 and UAV1–UAV2 must be 7.071 meters. Also, the distance between UAV1–UAV3, UAV2–UAV3, and UAV3–UAV4 is taken as 5 meters. For the second formation shape, the rhombus-shape formation is defined to provide an equal distance between the swarm members. To obtain this shape, the distance between UAV1, UAV2, UAV3, and UAV4 is taken 7.071 meters. As the third shape of formation, UAVs were asked to form formations in a line arrangement with equal distance between them. The desired distance between UAV1–UAV4, UAV1–UAV3, and UAV3–UAV2 is taken as 5 meters.

In Fig. 3(a), real-time distance information between UAVs during the triangular-shape formation flight is presented. Distance information shown in dark blue shows the change in distance between UAV1 and UAV3. First, it is seen that the distance between the two UAVs is 5 meters for the beginning. It is seen that the UAVs can maintain the distance between them with small changes throughout the formation flight and provide the desired 5 meters between them in the formation. Distance information given with the green line belongs to the distance change between UAV1 and UAV2. The initial distance between the two UAVs is seen to be approximately 16 meters. When the formation flight is realised, it has been observed that they have provided approximately 7.071 meters, which is the reference distance required between two UAVs in order to realise the triangle formation. Also, the red line gives the distance information between UAV2 and UAV3, and this distance is the longest distance between the UAVs when they are in the initial position. As can be understood from the distance information, it is observed that the UAVs approximately provided the desired 5-meter reference distance between them in order to provide the formation order by using their neighbour information. As can be seen from the remaining distance information between UAV1–UAV4, UAV2–UAV4, and UAV3–UAV4, it is observed that the UAVs share the distance and speed information among themselves thanks to the proposed controller and provide the desired reference distance between them for the triangle formation.

In Fig. 3(b), the distance errors that occur between the UAVs while forming the triangle formation shape are presented. The error information was obtained by using $\varepsilon_i=\sum_{j=1}^{N} a_{ij}\,(x_i-x_j-\delta_{ij})$ expression. For example, the distance error given by cyan reflects the distance error during formation flight between UAV1 and UAV3.

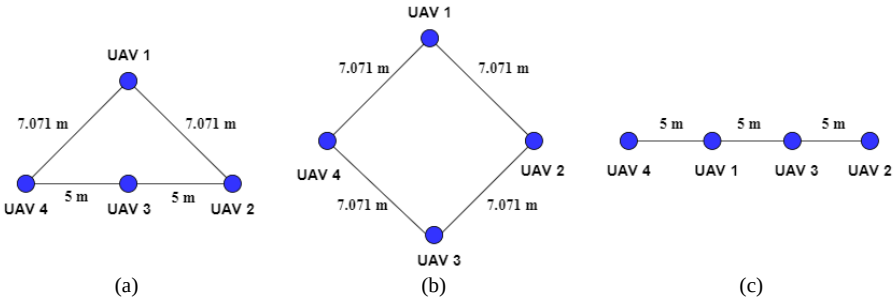

(a) (b) (c)

Fig. 2. Predefined formation shapes used in formation flights for swarm UAVs: (a) Triangular-shape formation; (b) Rhombus-shape formation; (c) Line-shape formation.

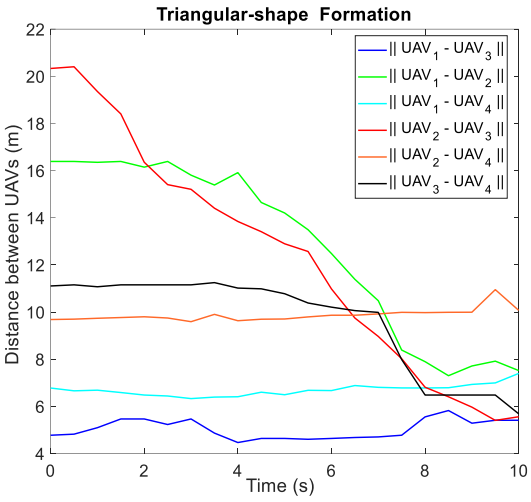

(a)

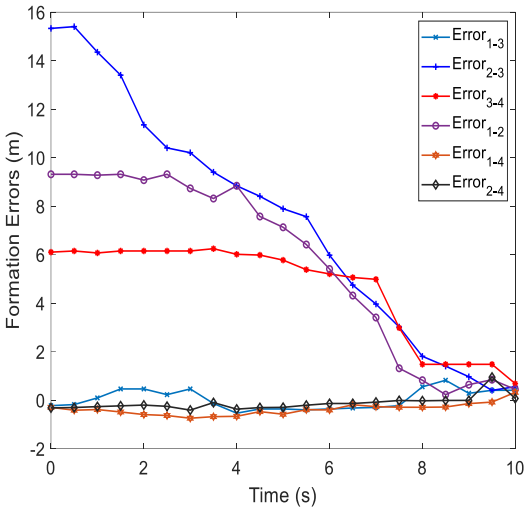

(b)

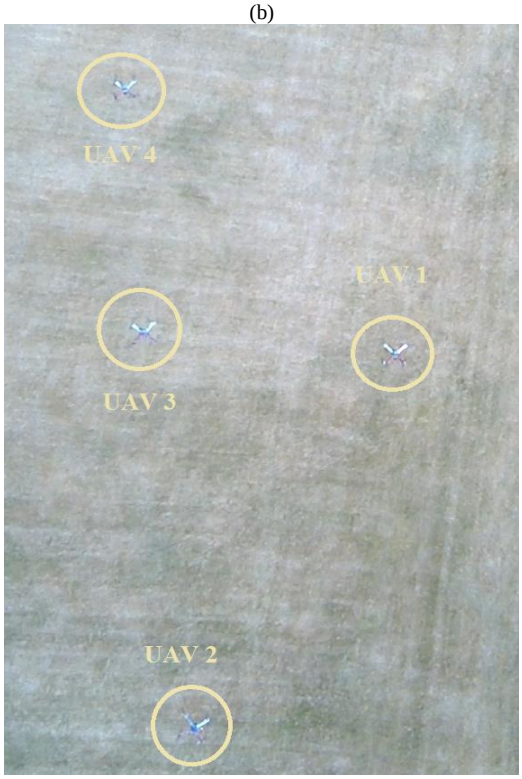

(c)

Fig. 3. (a) Distance information between UAVs during triangular-shape formation flight; (b) Distance error information between UAVs during triangular-shape formation flight; (c) Triangular-shape formation flight, image obtained in field tests of UAVs.

It means that the difference between actual distance ($x_i - x_j$) and the desired distance (δ_{ij}) is taken 5 meters between these UAVs. From the figure, one can understand that while realising the triangular-shape formation, it has been observed that the distance error between these two UAVs has varied within the range of about ±1 meter between 1st and 4th seconds. Afterwards, the formation error remained at nearly zero value until approximately 7.5th second. Then, although the error value increased between the 7.5th and the 9th seconds, it decreased again and converged to the nearly zero value due to the proposed controller, and this shows the effectiveness of the proposed controller as well. In addition, error changes between other UAVs during the triangular-shape formation flight can be observed on the same figure as well. When all error values are examined, it is seen that the formation distance error between all UAVs approaches zero value. Also, the real-time photo of the triangular-shape flight is presented in Fig. 3(c).

In Fig. 4(a), the real-time distance information between UAVs during the rhombus-shape formation flight is given. As can be seen from the figure, the largest distance change occurred between UAV1 and UAV 3 to maintain the relevant formation order. In addition, it has been observed that the UAVs in the swarm perform position verification during the formation flight and adjust the distance between them by moving back and forth when necessary (especially between 6–8 seconds). In Fig. 4(b), the distance error information between UAVs during rhombus-shape formation flight based on $\varepsilon_i = \sum_{j=1}^{N} a_{ij}(x_i - x_j - \delta_{ij})$ expression is presented. The reference distance between UAV1–UAV2–UAV3, and UAV4 is taken as δ_{ij} = 7.071 meters to create the formation of the rhombus-shape. As can be seen from the figure, the formation error variation between UAV2 and UAV4 is the least, on the other hand, the formation error variation between UAV1 and UAV3 is the highest. Moreover, when the formation errors obtained as a result of real-time tests are examined, it is seen that all error values are around ±0.6 meters. Also, the real-time photo of the rhombus-shape flight is presented in Fig. 4(c).

In Fig. 5(a), the real-time distance information between UAVs during the line-shape formation flight is given. It can be seen that the UAVs performed calm manoeuvres during line-shape formation, and it is observed that the difference in the distance indicated by the yellow line between the UAV3 and UAV4 is slightly higher than the other distance changes. In Fig. 5(b), the distance error information between the UAVs during the line-shape formation flight is given. To keep the UAVs in line formation, the desired distances between the UAV2–UAV3, UAV3–UAV1, and UAV1–UAV4 are taken as δ_{ij} = 5 meters. The most striking distance errors that occur during the line-shape formation flight are the error changes between UAV2–UAV3, UAV3–UAV4, and UAV1–UAV3. When looking at these changes, it is understood that UAVs are trying to eliminate distance errors between them by constantly verifying their location using the positions of their neighbours. Thus, the UAVs come to the right positions and also provide the desired

formation. However, when other error changes are examined, it can be clearly seen that the error values are not equal to zero, although the UAVs perform position verification based on the proposed controller. One of the reasons for these errors is that the GPS used on the UAVs cannot measure the distance very accurately. Moreover, the real-time photo of the line-shape flight is presented in Fig. 5(c).

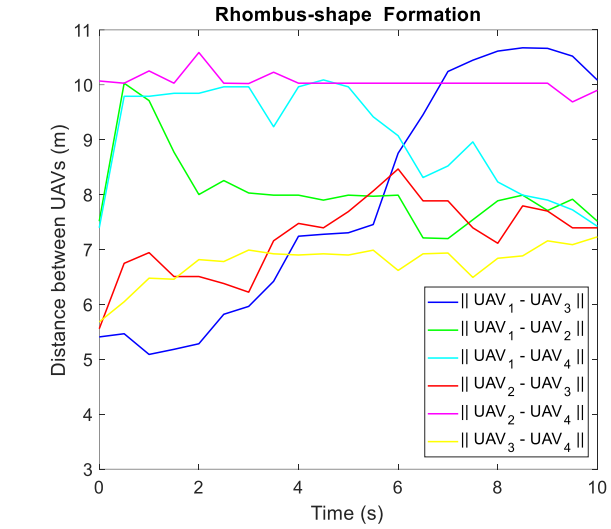

(a)

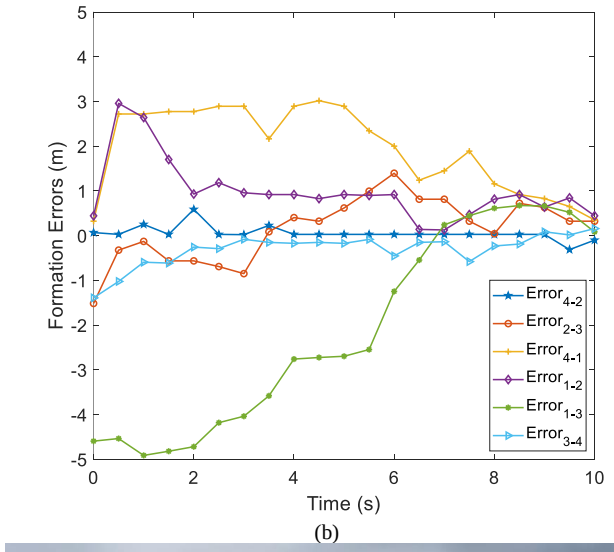

(b)

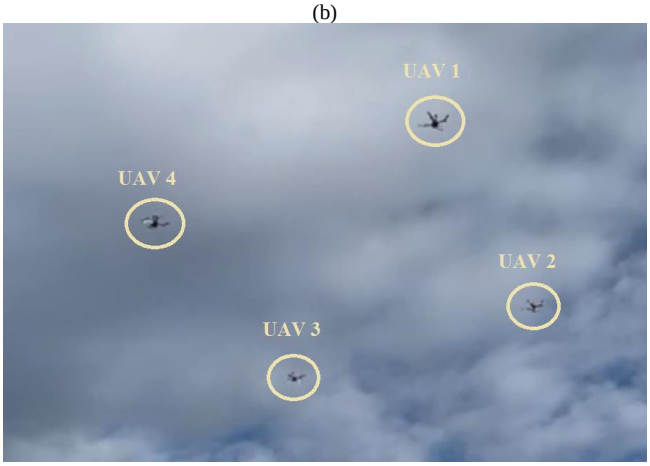

(c)

Fig. 4. (a) Distance information between UAVs during the rhombus-shape formation flight; (b) Distance error information between UAVs during the rhombus-shape formation flight; (c) Rhombus-shape formation flight image obtained in UAV field tests.

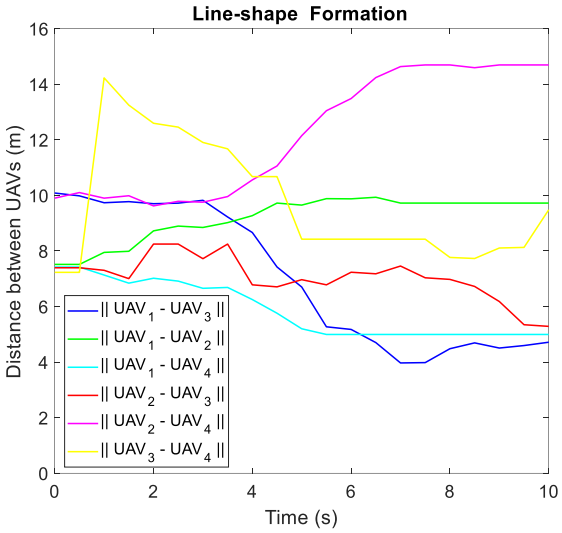

(a)

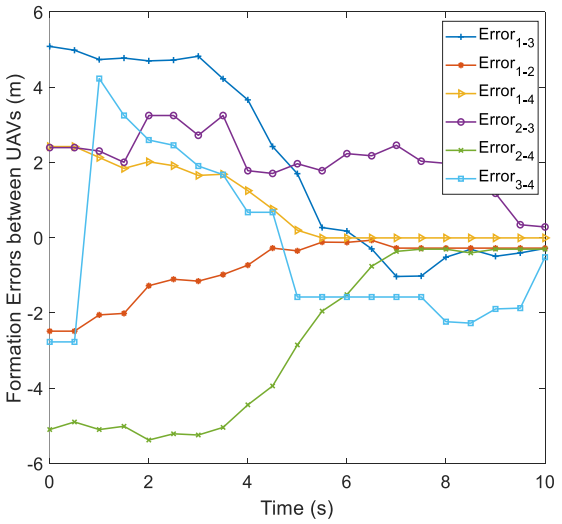

(b)

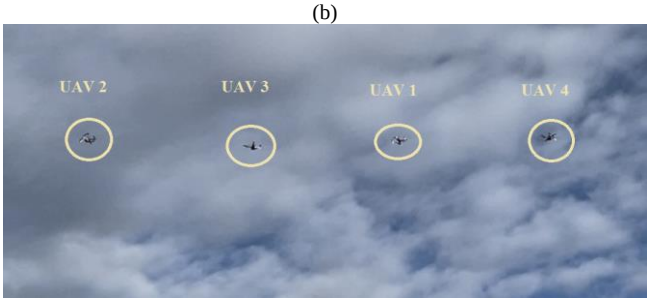

(c)

Fig. 5. (a) Distance information between UAVs during the line-shape formation flight; (b) Distance error information between UAVs during the line-shape formation flight; (c) Line-shape formation flight image obtained in UAV field tests.

V. CONCLUSIONS

In this paper, an R-CFC algorithm is proposed and tested to create triangular, rhombus, and line formations via a group of four-rotor UAVs in real-time outdoor experiment. First, four open source UAVs were designed and made ready to fly to carry out outdoor tests. Then, the proposed control algorithm was derived by taking into account basic consensus control algorithm, linear algebra, and graph theory as well. The experimental results show that the UAVs are able to realise predefined formation shapes very well, despite the measurement errors (nearly ± 50 cm) caused by GPS, thanks to the proposed R-CFC.

APPENDIX A

Lyapunov Stability Theorem

For a closed-loop system given in (6) under state feedback control is asymptotically stable in the sense of Lyapunov Stability Criteria, i.e., $x(t)\to 0$ as $t\to\infty$ for initial condition described as $x(t)|_{t=0}=x(0)$ apart from $x_0\neq 0 \Leftrightarrow$ if there exists a $\boldsymbol{P}$ matrix defined as $P=P^T>0$ such that [17]

$$(A-BK)^T P+P(A-BK)<0. \tag{A.1}$$

Proof: Consider a Lyapunov Candidate function described as given below [18]

$$V(x)=x^T Px. \tag{A.2}$$

Taking the time derivative of (A.2), one can obtain the following expression

$$\dot{V}(x)=\dot{x}^T Px+x^T P\dot{x}. \tag{A.3}$$

Substituting the closed-loop equation with state feedback $\dot{x}=(A-BK)x$ into (A.3), one gets

$$\dot{V}(x)=x^T\left[(A-BK)^T P+P(A-BK)\right]x, \tag{A.4}$$

and from (A.4), one can see that $\dot{V}(x)<0$ if and only if $(A-BK)^T P+P(A-BK)<0$ [19]. This means that the state described in (6) goes $x\to 0$ as $t\to\infty$. Hence, in order to stabilise an unstable system, the state feedback controller *K* must be selected that satisfies (A.1), and this ensures that the *(A - BK)* matrix is Hurwitz. However, to design a robust controller, the following equation should be examined under the condition $\mathrm{Re}(\lambda(A-\lambda_n BK))<0$ [14]

$$(A-\lambda_n BK)^T P+P(A-\lambda_n BK)<0. \tag{A.5}$$

If the above equation is written more clearly,

$$PA+A^T P-\lambda_n PBK-\lambda_n PB^T K^T<0 \tag{A.6}$$

is obtained. It is clear that the expression $PA+A^T P=\lambda_2 PBB^T P-Q$ can be obtained from the previously defined Riccati equation. After that, substituting this equation into (A.6) with the *K* gain given in (15), (16) is obtained and then the system is asymptotically stable.

CONFLICTS OF INTEREST

The authors declare that they have no conflicts of interest.

REFERENCES

[1] R. Rafifandi, D. L. Asri, E. Ekawati, and E. M. Budi, "Leader-follower formation control of two quadrotor UAVs", *SN Appl. Sci*., vol. 1, art. no. 539, 2019. DOI: 10.1007/s42452-019-0551-z.

[2] Y. Kuriki and T. Namerikawa, "Consensus-based cooperative formation control with collision avoidance for a multi-UAV system", in *Proc. of 2014 American Control Conference (ACC)*, 2014, pp. 2077–2082. DOI: 10.1109/ACC.2014.6858777.

[3] G. Lee and N. Y. Chong, "Decentralized formation control for small-scale robot teams with anonymity", *Mechatronics*, vol. 19, no. 1, pp. 85–105, 2009. DOI: 10.1016/j.mechatronics.2008.06.005.

[4] Y. Zou, Z. Zhou, X. Dong, and Z. Meng, "Distributed formation control for multiple vertical takeoff and landing UAVs with switching topologies", *IEEE/ASME Trans. on Mechatronics*, vol. 23, no. 4, pp. 1750–1761, 2018. DOI: 10.1109/TMECH.2018.2844306.

[5] K. Can and A. Basci, "Leader-follower formation control of quadrotors: A simple virtual leader approach", in *Proc. of 2nd Int. Sym. on App. Sci. and Eng. (ISASE2021)*, 2021, pp. 479–483.

[6] K. Fathian, T. H. Summers, and N. R. Gans, "Robust distributed formation control of agents with higher-order dynamics", *IEEE Control Systems Letters*, vol. 2, no. 3, pp. 495–500, 2018. DOI: 10.1109/LCSYS.2018.2841941.

[7] M. A. Toksöz, S. Oğuz, and V. Gazi, "Decentralized formation control of a swarm of quadrotor helicopters", in *Proc. of 2019 IEEE 15th Int. Conf. on Control and Automation (ICCA)*, 2019, pp. 1006–1013. DOI: 10.1109/ICCA.2019.8899628.

[8] R. T. Y. Thien and Y. Kim, "Decentralized formation flight via PID and integral sliding mode control", *Aerospace Sci. and Tech.*, vol. 81, pp. 322–332, 2018. DOI: 10.1016/j.ast.2018.08.011.

[9] X. Dong, B. Yu, Z. Shi, and Y. Zhong, "Time-varying formation control for unmanned aerial vehicles: Theories and applications", *IEEE Trans. Cont. Sys. Tech*., vol. 23, no. 1, pp. 340–348, 2015. DOI: 10.1109/TCST.2014.2314460.

[10] K. Can and A. Basci, "Time-varying consensus formation control of a group of quadrotor system with collision avoidance", in *Proc. of Int. Sym. on Unmanned Systems and the Defence Industry (ISUDEF'22)*, 2022.

[11] A. Basci, A. Derdiyok, K. Can, and K. Orman, "A fractional-order sliding mode controller design for tracking control of an unmanned aerial vehicle", *Elektronika ir Elektrotechnika*, vol. 26, no. 4, pp. 4–10, 2020. DOI: 10.5755/j01.eie.26.4.25846.

[12] L. Zhang, J. Wu, S. Liu, Z. Zhen, and X. He, "Equivalent sliding mode controller design based on "H" type quadrotor", in *Proc. of 2017 Int. Conf. on Mechanical, Sys. and Control Eng. (ICMSC)*, 2017, pp. 338–342. DOI: 10.1109/ICMSC.2017.7959497.

[13] Ş. G. Eski, "Normalleştirilmiş Laplacian ile işaretsiz Laplacian matrislerin özdeğerlei için sınırlar", M.S. thesis, Dept. Math., Ahi Evran Univ., Inst. of Sci., Kırşehir, Turkey, 2013.

[14] K. Can and A. Başçi, "Bir grup insansız hava aracının zamanla değişen yörünge boyunca konsensus tabanlı sürü kontrolü", *Fırat Üni. Uzay ve Savunma Teknolojileri Dergisi*, vol. 1, no. 1, pp. 441–446, 2022.

[15] W. Ren and R. W. Beard, *Distributed Consensus in Multi-Vehicle Cooperative Control: Theory and Applications*. Springer, 2008. DOI: 10.1007/978-1-84800-015-5.

[16] M. Xing, F. Deng, and Z. Hu, "Sampled-data consensus for multiagent systems with time delays and packet losses", *IEEE Trans. on Systems, Man and Cybernetics: Systems*, vol. 50, no. 1, pp. 203–210, 2020. DOI: 10.1109/TSMC.2018.2815616.

[17] M. Arcak, M. Larsen, and P. Kokotovic, "Circle and Popov criteria as tools for nonlinear feedback design", *Automatica*, vol. 39, no. 4, pp. 643–650, 2003. DOI: 10.1016/S0005-1098(02)00276-5.

[18] C.-F. Cheng, "Disturbances attenuation for interconnected systems by decentralized control", *Int. J. Control*, vol. 66, no. 2, pp. 213–224, 1997. DOI: 10.1080/002071797224702.

[19] W.-J. Mao and J. Chu, "Quadratic stability and stabilization of dynamic interval systems", *IEEE Trans. on Automatic Control*, vol. 48, no. 6, pp. 1007–1012, 2003. DOI: 10.1109/TAC.2003.812784.